Thermo-Optical modeling of hyperbolic cavity receiver of 40 m^2 parabolic dish collector

Pradipta Mandal, Abhinav Rajan, K. S. Reddy*

Heat Transfer and Thermal Power Laboratory, Department of Mechanical Engineering,
Indian Institute of Technology Madras, Chennai 600036, India

Abstract

Thermo-optical modeling of a solar cavity receiver, hyperbolic in shape, including a secondary reflector applicable for solar parabolic dish collector (PDC), is carried out in this article. The combined receiver and secondary reflector geometry constitute the hyperbolic shape. This investigation aims to optimize the receiver geometrically and optically, then to estimate the heat transfer rate from the receiver surface owing to natural convection and radiation of the optimized receiver under parameters that influence the PDC system performance. The commercial optical software tool ASAP® 2013 is used for optical simulation. The optical simulation includes the investigation of the performance of the receiver for varying cavity height h_1 and secondary height h_2 at a constant diameter of the cavity aperture of d = 0.5 m. The effects of cavity absorptivity (86-94%) and reflectivity of the secondary (86-94%) on optical performance are also studied. The optimal value of optical efficiency found is 91.72% for the mounting height of 4.21 m when h_1= 0.75 m and h_2 = 0.25 m. With ANSYS® Fluent 2020 R1, the receiver's 0°, 30°, 60°, and 90° orientations or angle of tilt θ are modeled thermally. A thorough analysis comparing the various turbulence models has been presented.

Keywords: Parabolic dish collector, Cavity receiver, Optical simulation, Thermal simulation, Geometrical concentration ratio, Secondary trumpet

* Corresponding author. E-mail address: ksreddy@iitm.ac.in (K.S. Reddy)

10.18086/swc.2023.03.07 Available at http://proceedings.ises.org

1 Introduction

Since fossil fuels are exhaustible and responsible for polluting the environment, technologies for converting solar energy into thermal energy are becoming more and more popular. The solar parabolic dish system is one concentrating solar power (CSP) technology that shows promise for effective solar-thermal energy conversion. The essential elements of a Parabolic Dish Collector (PDC) system, a point-focused technology, include the concentrator, receiver, dual-axis tracking system, and supporting structure. The cavity's geometry is essential and affects the system's overall performance.

Many researchers have analyzed heat loss for cavity receivers of various shapes, such as cylindrical, hemispherical, conical, etc. Pavlovic et al. (2018) compared conical with spiral-shaped receivers experimentally. Bellos et al. (2019) have examined various cavity receiver forms from both the optical and thermal points of perspective. Their results indicate that the cylindrical-conical design geometry is the ideal one. Taumoefolau et al. (2004) conducted experiments at different inclination angles and aperture-to-cavity diameter ratios to ascertain the heat lost via free convection from dish cavity geometry form. Johnston (1998) measured and defined a 20 m^2 dish's focal zone experimentally. Daabo et al. (2016a) focused on the distribution of flux and optical performance for various receiver shapes, such as conical, spherical, and cylindrical ones. Si-Quan et al. (2019) evaluated the optical performance (88.9%) of a spherically shaped cavity receiver using the Monte Carlo Ray Tracing (MCRT) method. An additional and workable strategy to amplify the efficiency of the solar energy-to-thermal energy transformation process is to minimize the radiation heat loss from a receiver and optimize the receiver's geometry and shape. It has been demonstrated by Ngo et al. (2015) that heat loss from natural convection can be minimized by plate fins fastened to a cavity. The wind speed, direction, and receiver inclination significantly affect heat loss. López et al. (2020) reported the thermal performances of flat and cavity-type receivers for industrial applications. Reddy et al. (2016) have investigated the effect of different operating wind velocities and directions on heat loss for modified cavity receivers tiled at different angles. Craig et al. (2020) analyzed the heat loss from a tubular receiver. Using thorough ray tracing simulations, Hernández et al. (2012) designed a unique type of receiver and optimized with a large rim angle of 90°. The dimensions of cylindrical, conical, and spherical cavities are compared and optimized.

A parabolic dish with a second-stage optical feature can improve the concentration ratio at a fixed interception factor. Making use of a secondary reflector for increasing the concentration level can be beneficial if the first reflector has a significant error and a high required temperature (Jaffe and Poon, 1981). Wang et al. (2020) investigated the improvement in the performance of cavity receiver geometry with spilled skirts using hyperbolic trumpet, compound parabolic concentrator (CPC), and conical as secondary. The MCRT is used to assess the cavity receivers' efficacy using heat transfer models. Reddy and Kumar (2009) developed a computer model for the modified cavity receiver that considers radiation and evaluates the convection-owned heat loss with reflectors that have conical-type, CPC-type, and trumpet-type forms. The authors reported that the solar receiver with the hyperbolic trumpet as secondary performed better than the receiver with CPC and conical.

One of the critical elements in transforming solar energy into thermal is designing the receiver with a suitable geometry. The shape and angle of the cavity's tilt affect the total performance, which impacts heat loss. The current study improves the concentration ratio by attaching a hyperbolic secondary concentrator, which raises the receiver's surface temperature and enhances system performance overall. This paper offers a detailed investigation using optical-coupled-thermal modeling of a parabolic dish concentrator's hyperbolic cavity-type receiver.

2 System configuration

The PDC of aperture 40 m^2 and receiver analyzed in this work are illustrated in Fig. 1. The receiver geometry is produced in SolidWorks 2019. The maximum concentration is achieved for the rim angle ϕ of 45° (Bopche and Kumar, 2019). Therefore ϕ = 45° is taken in this analysis, for which, the focal length f is calculated to be 4.31 m. The hyperbolic profile is created by both the cavity and trumpet secondary, which are attached. The geometry on which optimization is performed has aperture diameter d = 0.5 m and dimeter-to-total height ratio d/h = 1. The total height h of the geometry is the sum of the cavity height (h_1) and the secondary reflector height h_2; h_1 and h_2 are equal. The absorptivity α_{rec} of receiver surface, reflectivity (ρ_{sec}) of the secondary as well as mounting height L are optimised. The concentrator surface is thought to feature a glass mirror and an iron-silver coating. The position of the receiver is on the PDC's focal plane. The ideal installation height L is attained by vertical movement of the receiver from the base of the concentrator.

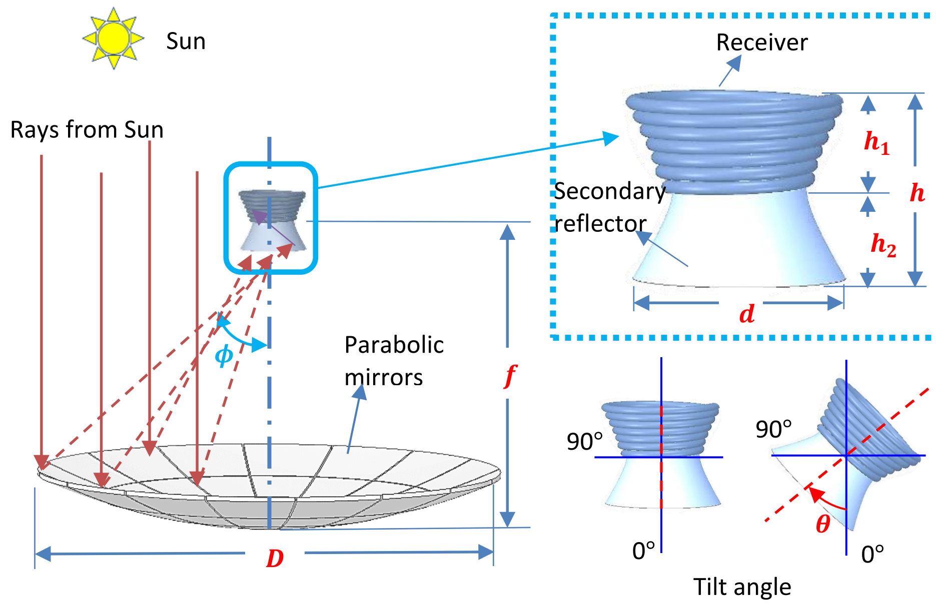

Fig. 1. Dish-receiver system.

As shown in Fig. 1, sunlight falls in a parallel beam across the entire dish area, focusing on the secondary. This is the initial focus phase, and the parabolic dish is appropriately referred to as a primary concentrator. The concentrated ray is then reflected once more onto the cavity from the secondary, which absorbs solar radiation as the second step of concentration.

3 Optical model

The optical model for analyzing the receiver is built using the commercial tool ASAP® 2013 and simulated using the technique of Monte Carlo Ray Tracing (MCRT). The direct normal irradiance (DNI) of 800 W/m^2 impinges on the dish aperture. The reflectivity ρ_{dish} of the dish surface and the secondary reflector ρ_{sec} are 92% and 94%, respectively. The absorptivity α_{rec} value of 94% is assigned to the surface of the cavity. The heat absorbed over the inside surface is considered to calculate the absorbed heat and, ultimately, the optical efficiency. To dimensionally optimize, a parametric simulation of the receiver is done by changing h_1 when d and h_2 are constant and then changing h_2 when d and h_2 are maintained at a constant value. Due to the change in h_1 and h_2, the total height h changes. This leads to a variation of d/h as 0.5, 1, and 1.5.

The sun is defined as an extended source. The source is modeled as an emitting disk. The emitting disk simulates a simple Lambertian surface emitter with elliptical boundaries and a divergence half angle of 0°, which refers to the collimated beam. The source model in ASAP is characterized by randomness.

The relation for focal length f, which is the length between the collector base and its focal point, in terms D and ϕ, is given as follows:

$$f = \frac{D}{4\,tan\,(\frac{\varphi}{2})} \quad \text{(eq. 1)}$$

The current optical simulation assumes perfect optics, implying that different optical errors (errors due to sun shape, tracking, specularity, and slope) are considered negligible (Daabo et al., 2016b).

The solar irradiation captured by the collector aperture Q_{dish} is obtained as (Bellos et al., 2019):

$$Q_{dish} = A_{dish} \times DNI \quad \text{(eq. 2)}$$

where, A_{dish} is the collector aperture area.

Then, optical efficiency ($\eta_{optical}$) is defined as the fraction of the radiative energy falling over the collector's aperture surface that is ultimately absorbed by the receiver surface (Q_{rec}) and it is expressed as:

$$\eta_{optical} = \frac{Q_{rec}}{Q_{dish}} \quad \text{(eq. 3)}$$

3.1 Ray sensitivity test and validation

One million have been chosen for simulation after the ray sensitivity test because there is practically no change in optical efficiency as the ray count number crosses one million. The ray tracing is demonstrated in Fig. 2(a). The validity of the present optical model is established against the experiment data of Johnston (1998). Here, the author reported the distribution of radiant flux at the PDC system's focal region, which has an aperture area of 20 m^2. A 0.5 m diameter circular copper target was positioned at the focal region. The flux distribution estimated using the present model is compared with that of the literature and is depicted in Fig. 2(b). Further, the model utilized to calculate the total power at the receiver is also validated against the published data literature (Daabo et al., 2016a). The maximum difference in total power results is 7.73%.

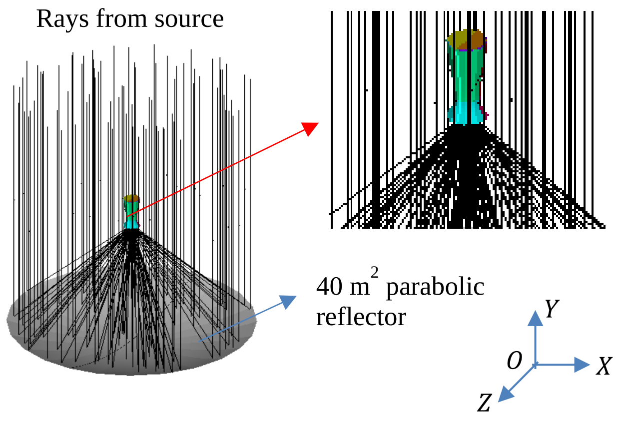

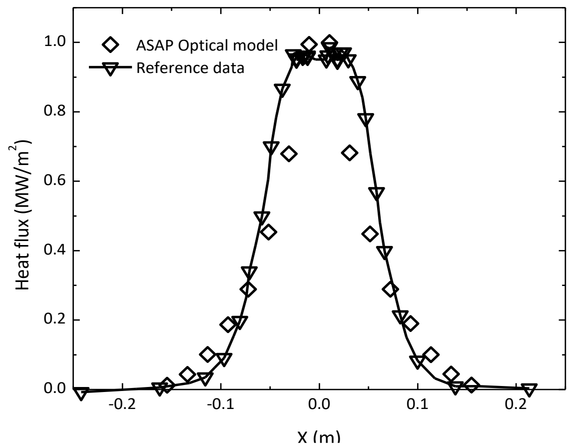

Fig. 2. (a) Ray tracing of solar PDC (b) Validation of flux intensity distribution between against experimental data (Johnston, 1998).

4 Thermal model

4.1 Governing equation

The continuity, momentum, and energy equations regulating laminar natural convection are solved successively (eqs. 4-6):

Continuity equation: $$\nabla V_{vel} = 0 \quad \text{(eq. 4)}$$

Momentum equation: $$V_{vel}\nabla V_{vel} = X - \frac{\nabla p}{\rho_f} + \nu\nabla^2 V_{vel} \quad \text{(eq. 5)}$$

Energy equation: $$\nabla(k_s \nabla T) = 0 \quad \text{(eq. 6)}$$

where ∇ is the Laplace operator, V_{vel} denotes velocity (m/s), p represents pressure (Pa), T indicates temperature (K), ν denotes kinematic viscosity (m^2/s), k_s is thermal conductivity (W/m.K) and X is body force (N/m^3).

The thermal model involves the following assumptions: (1) no wind velocity exists. (2) The receiver surface temperature equals the fluid temperature. (3) The tubular coil of the receiver is so closely packed that it forms a continuous and smooth surface.

The surrounding air is taken to be an ideal, incompressible gas. Density of the air ρ_f is specified using this assumption as:

$$\rho_f = \frac{P_{op}}{RT/M_w} \quad \text{(eq. 7)}$$

where, P_{op} is the operating pressure and M_w is the molecular weight. P_{op} is constant and does not depend on the local relative pressure field value.

The steady-state equations are solved with the Fluent solver. A non-Boussinesq approximation is used to solve the momentum equations. It is appropriate to use the Boussinesq approximation if $\beta(T_w - T_\infty) \ll 1$, where β is the coefficient of thermal expansion, T_w and T_∞ are receiver wall temperature and the ambiance temperature. Because of the secondary, the wall surface receivers are subjected to significant heat flux and reach high surface temperatures. It is, therefore, anticipated that the non-Boussinesq model will be more suitable than the Boussinesq model.

The surface-to-surface (S2S) radiation model is used to calculate surface radiation. Reflected flux refers to the radiant flux coming from the environment, which is interpreted as the radiation that exits all the other surfaces. The eqs. (8-10) below represent the energy that gets reflected from the surface i (Reddy and Sendhil Kumar, 2009):

$$q_{out,i} = \varepsilon_i \sigma T_i^4 + (1 - \alpha_i) q_{in,i} \quad \text{(eq. 8)}$$

$q_{in,i}$ is represented in terms of $q_{out,j}$ as

$$q_{out,i} = \varepsilon_i \sigma T_i^4 + (1 - \alpha_i) \sum_{j=1}^{N} F_{ij} q_{out,j} \quad \text{(eq. 9)}$$

The above equation can also be expressed as:

$$J_i = E_i + (1 - \alpha_i) \sum_{j=1}^{N} F_{ij} J_j \quad \text{(eq.10)}$$

where, J_i is the radiosity (W/m^2), F_{ij} is the shape factor from surface i to j, $\sigma = 5.67 \times 10^{-8}$ W/m^2.K^4 denotes the Stefan-Boltzmann constant, E_i is emissive power at surface i (W/m^2), and N is the number of radiative surfaces.

4.2 Model selection and validation

The validity of the thermal model is supported by the experimental findings in the literature (Taumoefolau et al., 2004), as shown in Fig.3(a). According to this research, natural convection losses from cavity-type receivers were studied using an electrically heated receiver. The analysis was conducted at angles ranging from -90° (aperture facing upward) to 90° (aperture facing downward), and temperatures between 450°C and 650°C were examined. Computational predictions of convection losses from the cavity were made for the angles from 0° to 90°. A reasonable variation exists between the experiment's outcomes and those from the current model. Moreover, the chosen model has also been contrasted with other models, such as laminar, SST $k - \omega$, and realizable $k - \omega$. Fig.3(b) presents a comparison of the acquired data. The laminar model is found to have significantly good prediction.

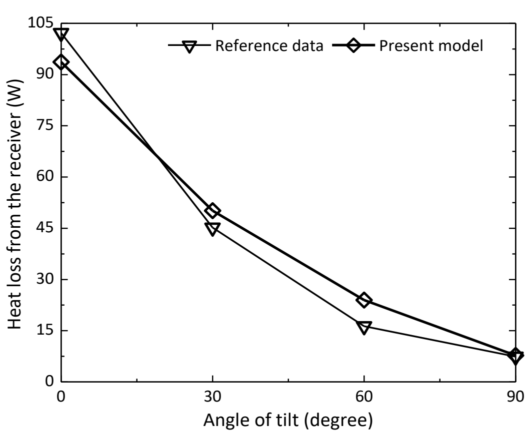

(a)

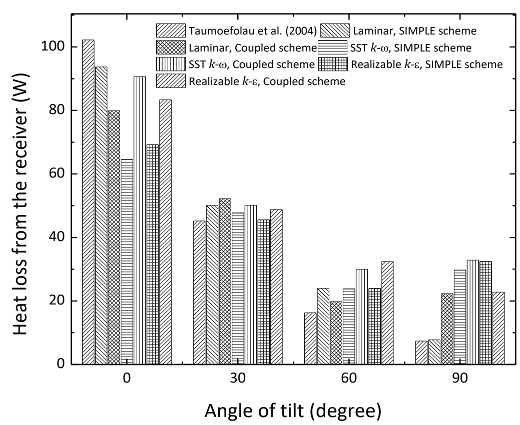

(b)

Fig. 3. (a) Validation of thermal model with experiment (b) comparison of different turbulent models with various schemes for pressure-velocity coupling.

4.3 Numerical procedure

The geometry was divided into eleven parts following the ray tracing analysis to obtain more precise results for the radiative flux. The optical simulation is used to retrieve each element's absorbed heat data. These values have been applied at each element's inner surface as boundary conditions for a constant heat flux. After that, ANSYS® Fluent

2020 R1 is used to import the model geometry and mesh the problem. The receiver is situated inside the suitably sized cylindrical domain. A cylindrical enclosure was selected, and its size was increased so that its impact on thermo-fluidic analysis became negligible and had no discernable influence on the heat transfer rate. A steady-state model and a pressure-based solver are employed in the thermal model. For numerical analysis, the tilt angle has been changed from 0° to 90°, with 0° representing the receiver's upright position.

4.4 Grid sensitivity test and implemented boundary conditions

The inside surfaces of the receiver are subjected to constant heating because they are continuously exposed to solar radiation. As a result, boundary conditions of constant heat flux (radiative flux) values, as determined by optical simulation, have been applied to the cavity's interior wall. It is presumed that ceramic wool insulation covers the outside surface to stop heat transfer to the surrounding air. Thus, the external cavity surface is subjected to the adiabatic boundary conditions. The hyperbolic receiver can be considered surrounded by an unbounded atmosphere. As a result, the domain's pressure inlet is designated as the border condition. It is believed that the surrounding air is a perfect, incompressible gas. The properties of air are modeled as polynomial temperature functions applicable from 300 K to 1000 K. Due to the intricate shape of the receiver, the governing equations (eqs. 4-6) are discretized using an unstructured polyhedral mesh. The air inside the cavity is the working fluid. The Semi-Implicit Method for Pressure Linked Equations (SIMPLE) scheme is employed to couple the pressure and velocity terms. The continuity, momentum, and energy equations were set to 10^{-3}, 10^{-3}, and 10^{-6} as convergence residuals, respectively. The grid independence test involves systematically increasing the number of cells and decreasing cell sizes to ensure the heat loss from the internal region of the cavity is accurately captured without discrepancies as the grid resolution increases. The mesh with 583,533 cells is determined to be the optimal size for meeting accuracy requirements. Fig. 4 shows the volume mesh of the domain and the receiver.

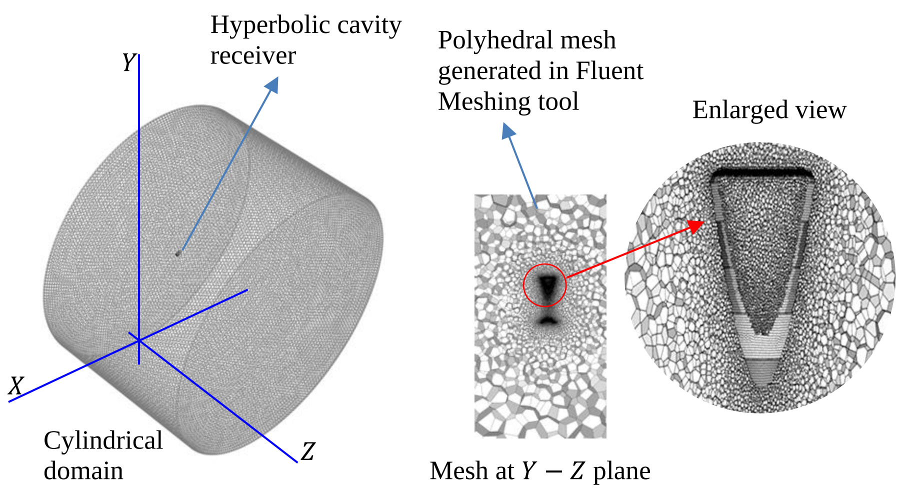

Fig. 4. Meshing of computational domain and receiver.

5 Results and discussion

The cavity receiver, hyperbolic in shape, that has an attached secondary for a 40 m^2 PDC system, is optically optimized by parametric optical modeling. Subsequently, a thermal simulation is performed to determine the area-weighted average temperature and heat loss via convection and radiation. This section includes the effect of diameter-to-height ratio, absorptivity, reflectivity, and inclination.

5.1 Effects of cavity height (h_1) and secondary height (h_2)

The optical efficiency of the system varies with position. Specifically, only h_2 is systematically adjusted, leading to changes in h. Additionally, the diameter of the circular aperture remains constant at all points of interest. The optical efficiency is assessed for various mounting positions ranging from 4.21 to 4.41 m, with increments or decrements of 0.05 m across different d/h ratios. It is evident from Fig. 5(a) that the maximum optical efficiency occurs at $L = 4.21$ m when $h_1 = 0.75$ m and d/h = 0.5. This occurs because raising the secondary height enables greater radiation for the second-stage concentration. Fig. 5(b) shows that when h_2= 0.75 m, the optical efficiency hits the highest value. Therefore, increasing the secondary height leads to improved receiver performance at a greater mounting height.

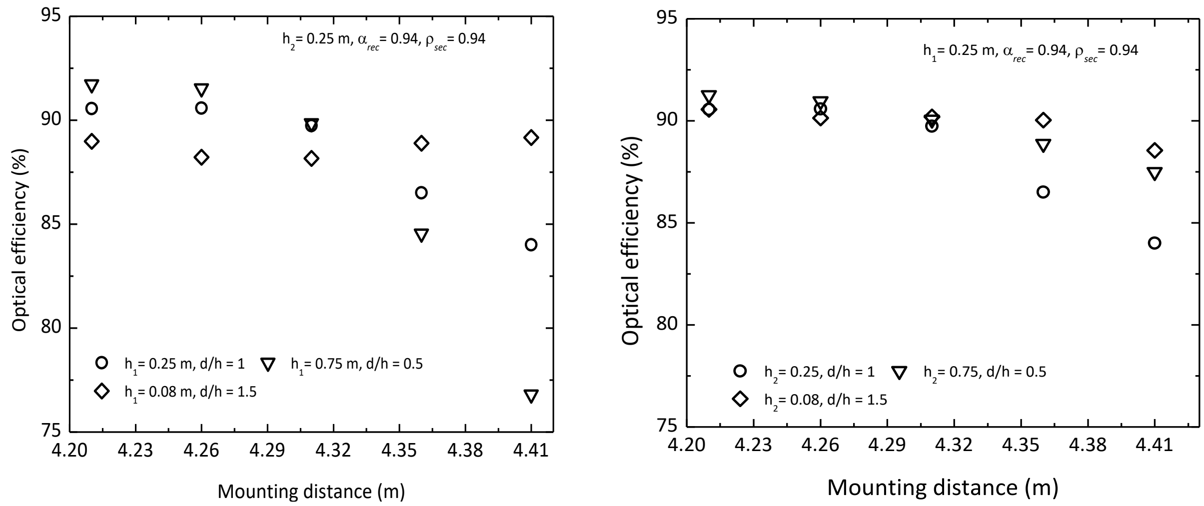

(a) (b)

Fig. 5. Variation of optical efficiency with mounting height at different (a) cavity heights (h_1) and (b) secondary height (h_2).

5.2 Variation of optical performance with wall absorptivity (α_{rec}) and secondary reflectivity (ρ_{sec})

Fig. 6(a) illustrates how optical performance varies with mounting height for different absorptivity values. A range of absorptivity α_{rec} = 86-94% has been examined to study parametrically. The reflectivity value is held constant at ρ_{sec} = 94%. From Fig. 6(a), it's clear that optical efficiency decreases as mounting height increases but increases with higher absorptivity. In other words, higher absorptivity leads to higher optical efficiency. Fig. 6(b) shows how optical efficiency changes with mounting height for various reflectivity values. The range of reflectivity values considered for the analysis is ρ_{sec} = 86-94%. The absorptivity value is held constant at α_{rec} = 94%. It is noted that optical efficiency decreases as mounting height increases. Unlike absorptivity, optical efficiency decreases with higher reflectivity values. Additionally, a comparison of the optical performance of the current receiver with existing studies is presented in Table 1.

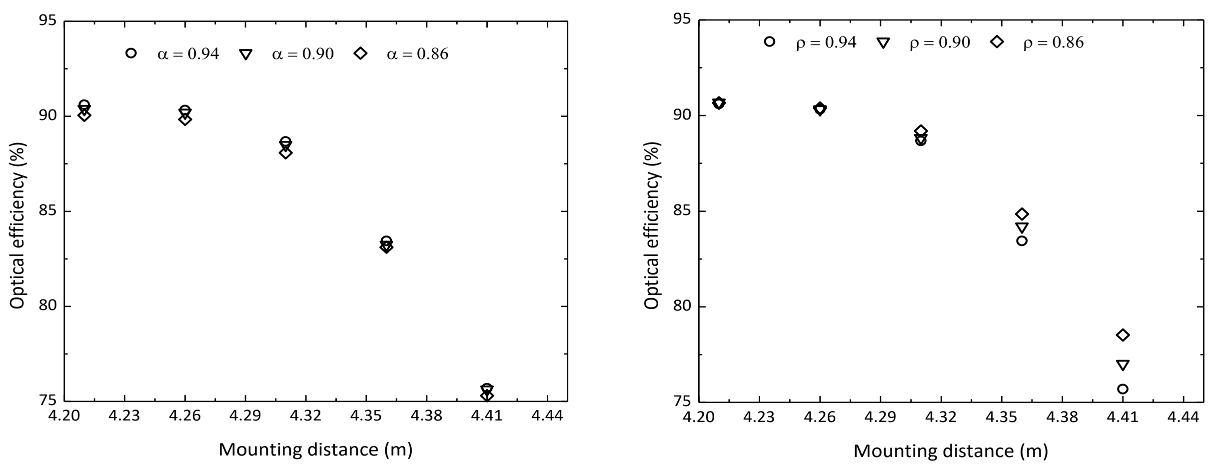

(a) (b)

Fig. 6. Variation of optical efficiency with mounting height for different (a) receiver wall absorptivity (α_{rec}) and (b) reflectivity of secondary (ρ_{sec}).

Table 1 Comparative tabulation of the optical performance of the proposed receiver.

References	Receiver geometry	Maximum optical efficiency (%)
Daabo et al. (2016b)	Conical	75.3
Bellos et al. (2019)	Cylindrical	81.34
	Rectangular	80.11
	Spherical	78.78
	Conical	80.96
Hassan et al. (2021)	Cylindrical	80
Si-Quan et al. (2019)	Spherical	88.9
Proposed receiver	Hyperbolic cavity receiver with secondary	91.72

5.3 Effect of tilt angle (θ) of receiver

Fig. 7(a) and (b) illustrate the relationship between the rate of heat loss from radiation and free convection with the tilt angle for an emissivity (ε) from 0.2 to 1.0. The convective heat loss rises with the receiver tilt. However, because of the numerical model's constant heat flux boundary conditions, radiation heat loss shows the opposite trend. The convective heat loss rises with tilt angle while radiative heat loss decreases. The stagnant zone diminishes, and the convection zone expands as the tilt changes from 0° to 90°. Hot air within the secondary reflector and cavity decreases progressively as the tilt changes from 0° to 90° (Rajan and Reddy, 2021). As the receiver's tilt angle varies from 0° to 90°, the stagnation zone of the receiver gradually decreases. At a tilt of 0°, the stagnant zone occupies most of the space within the cavity receiver. Therefore, the convective heat loss rate rises as the tilt increases.

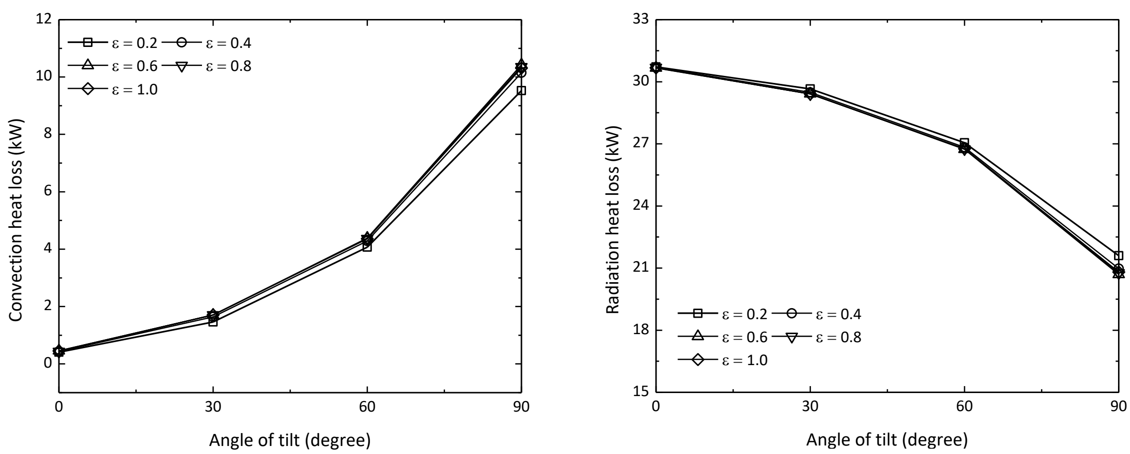

(a) (b)

Fig. 7. Effect of tilt on heat loss (a) via convection (b) radiation.

6 Conclusions

The study is conducted on a 40 m^2 PDC system's hyperbolic cavity receiver, employing ray tracing alongside a thermal model. The receiver's comprehensive optical simulation was carried out using the Monte Carlo Ray Tracing (MCRT) method. The optical modeling is conducted for receivers with different d/h values (0.5−1.5), along with secondary reflectors of varying heights (h_2= 0.08-0.75 m). The highest optical efficiency observed is 91.72% when d/h is 0.5 at a mounting height of 4.21 m. Subsequently, the performance is evaluated for different receiver absorptivity values (0.86-0.94) and secondary reflectivity values (86-94%). With α_{rec} = 94% and ρ_{sec} = 86%, the receiver exhibited optimal performance at a mounting height of 4.21 m. The thermal simulation indicates that convection heat transfer increases as the angle of tilt θ is changed from 0° to 90°, while radiation heat transfer decreases within the emissivity range of ε = 0.2-1.0.

References

Bellos, E., Bousi, E., Tzivanidis, C., Pavlovic, S., 2019. Optical and thermal analysis of different cavity receiver designs for solar dish concentrators. Energy Convers. Manag. X 2, 100013. https://doi.org/10.1016/J.ECMX.2019.100013

Bopche, S.B., Kumar, S., 2019. Experimental investigations on thermal performance characteristics of a solar cavity receiver. Int. J. Energy Environ. Eng. 10, 463–481. https://doi.org/10.1007/s40095-019-00321-4

Craig, K.J., Slootweg, M., Le Roux, W.G., Wolff, T.M., Meyer, J.P., 2020. Using CFD and ray tracing to estimate the heat losses of a tubular cavity dish receiver for different inclination angles. Sol. Energy 211, 1137–1158. https://doi.org/10.1016/j.solener.2020.10.054

Daabo, A.M., Mahmoud, S., Al-Dadah, R.K., 2016a. The optical efficiency of three different geometries of a small scale cavity receiver for concentrated solar applications. Appl. Energy 179, 1081–1096. https://doi.org/10.1016/j.apenergy.2016.07.064

Daabo, A.M., Mahmoud, S., Al-Dadah, R.K., 2016b. The effect of receiver geometry on the optical performance of a small-scale solar cavity receiver for parabolic dish applications. Energy 114, 513–525. https://doi.org/10.1016/J.ENERGY.2016.08.025

Hassan, A., Quanfang, C., Abbas, S., Lu, W., Youming, L., 2021. An experimental investigation on thermal and optical analysis of cylindrical and conical cavity copper tube receivers design for solar dish concentrator. Renew. Energy 179, 1849–1864. https://doi.org/10.1016/j.renene.2021.07.145

Jaffe, L.D., Poon, P.T., 1981. Secondary Concentrators for Parabolic Dish Solar Thermal Power Systems. Proc. Intersoc. Energy Convers. Eng. Conf. 2, 1752–1758.

Johnston, G., 1998. Focal region measurements of the 20 m2 tiled dish at the Australian National University. Sol. Energy 63, 117–124. https://doi.org/10.1016/S0038-092X(98)00041-3

López, O., Baños, A., Arenas, A., 2020. On the thermal performance of flat and cavity receivers for a parabolic dish concentrator and low/medium temperatures. Sol. Energy 199, 911–923. https://doi.org/10.1016/J.SOLENER.2019.07.056

Ngo, L.C., Bello-Ochende, T., Meyer, J.P., 2015. Numerical modelling and optimisation of natural convection heat loss suppression in a solar cavity receiver with plate fins. Renew. Energy 74, 95–105. https://doi.org/10.1016/j.renene.2014.07.047

Pavlovic, S., Loni, R., Bellos, E., Vasiljević, D., Najafi, G., Kasaeian, A., 2018. Comparative study of spiral and conical cavity receivers for a solar dish collector. Energy Convers. Manag. 178, 111–122. https://doi.org/10.1016/J.ENCONMAN.2018.10.030

Rajan, A., Reddy, K.S., 2021. Estimation of convective heat losses from conical cavity receiver of solar parabolic dish collector under wind conditions and receiver orientations. E3S Web Conf. 313, 11001. https://doi.org/10.1051/e3sconf/202131311001

Reddy, K.S., Sendhil Kumar, N., 2009. Convection and surface radiation heat losses from modified cavity receiver of solar parabolic dish collector with two-stage concentration. Heat Mass Transf. und Stoffuebertragung 45, 363–373. https://doi.org/10.1007/S00231-008-0440-2

Reddy, K.S., Veershetty, G., Srihari Vikram, T., 2016. Effect of wind speed and direction on convective heat losses from solar parabolic dish modified cavity receiver. Sol. Energy 131, 183–198. https://doi.org/10.1016/j.solener.2016.02.039

Si-Quan, Z., Xin-Feng, L., Liu, D., Qing-Song, M., 2019. A numerical study on optical and thermodynamic characteristics of a spherical cavity receiver. Appl. Therm. Eng. 149, 11–21. https://doi.org/10.1016/j.applthermaleng.2018.10.030

Taumoefolau, T., Paitoonsurikarn, S., Hughes, G., Lovegrove, K., 2004. Experimental investigation of natural convection heat loss from a model solar concentrator cavity receiver. J. Sol. Energy Eng. Trans. ASME. https://doi.org/10.1115/1.1687403

Wang, S., Asselineau, C.-A., Wang, Y., Pye, J., Coventry, J., 2020. Performance enhancement of cavity receivers with spillage skirts and secondary reflectors in concentrated solar dish and tower systems. Sol. Energy 208, 708–727. https://doi.org/10.1016/j.solener.2020.08.008